Supporting information

Quasi-BIC-empowered integrated sensing dielectric metasurface for molecular fingerprint retrieval and chiral detection

Yuhang Wei[1], Liming Si[1], Kunlin Han[2], Haoyan Xu[1], Xiue Bao[1], Weiren Zhu[3*]*

[1] Beijing Key Laboratory of Millimeter Wave and Terahertz Technology, School of Integrated Circuits and Electronics, Beijing Institute of Technology, Beijing 100081, China.

[2] School of Cyberspace Security, Beijing Institute of Technology, Beijing 100081, China.

[3] Department of Electronic Engineering, Shanghai Jiao Tong University, Shanghai 200240, China;

S1. Quasi-BIC modes of the metasurface under TM polarization excitation

Under TM excitation, the metasurface also supports similar Quasi-BIC modes driven by gap perturbation, with the Q factor being inversely proportional to the square of the asymmetry parameter α_0, which are presented in Figure S1

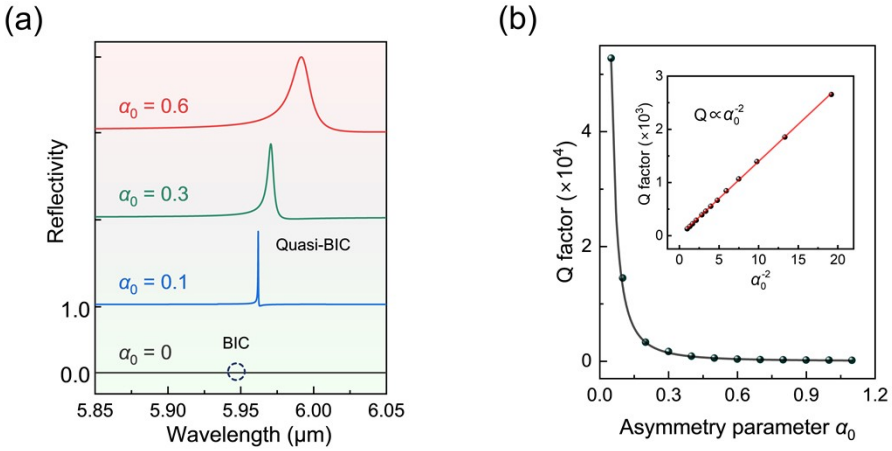

Figure S1. (a) Reflection spectra for different asymmetry parameter α_0 under TM excitation. (b) Dependence of the Q factors on the α_0 under TM excitation, and the inset shows the linear fitting between Q and α_0^{-2}.

S2. Details for multipole expansion

The multipole expansion of the near field is obtained by integrating the charge density ρ(**r**) and current density **J**(**r**) distributions within the unit cell in Cartesian coordinate. The higher order of the multipole moments such as electromagnetic octupoles and toroidal quadrupoles are relatively minor and generally not taken into account. Therefore, we primarily calculate the electric dipole (ED), magnetic dipole (MD), electric quadrupole (EQ), magnetic quadrupole (MQ), and toroidal dipole (TD), which can be calculated as follows[40]

$$P = \frac{1}{i\omega}\int_V \boldsymbol{J}(\boldsymbol{r})d\boldsymbol{r}$$

$$M = \frac{1}{2c}\int_V [\boldsymbol{r}\times\boldsymbol{J}(\boldsymbol{r})]d\boldsymbol{r}$$

$$T = \frac{1}{10c}\int_V \left[(\boldsymbol{r}\cdot\boldsymbol{J}(\boldsymbol{r}))r - 2r^2\boldsymbol{J}(\boldsymbol{r})\right]d\boldsymbol{r}$$

$$EQ_{\alpha\beta} = \frac{1}{2i\omega}\int_V \left[(r_\alpha J_\beta + r_\beta J_\alpha) - \frac{2}{3}\delta_{\alpha\beta}(\boldsymbol{r}\cdot\boldsymbol{J}(\boldsymbol{r}))\right]d\boldsymbol{r}$$

$$MQ_{\alpha\beta} = \frac{1}{3c}\int_V \left\{[\boldsymbol{r}\times\boldsymbol{J}(\boldsymbol{r})]_\alpha r_\beta + [\boldsymbol{r}\times\boldsymbol{J}(\boldsymbol{r})]_\beta r_\alpha\right\}d\boldsymbol{r}$$

where $i\omega\rho(\boldsymbol{r}) + \mathrm{div}\boldsymbol{J}(\boldsymbol{r}) = 0$, $\delta_{\alpha\beta}$ is the delta function, and $\alpha,\beta = x,y,z$. The far field

scattering intensity of each electromagnetic multipole can be written as:

$$I_P = \frac{2\omega^4}{3c^3}|P|^2$$

$$I_M = \frac{2\omega^4}{3c^3}|M|^2$$

$$I_T = \frac{2\omega^6}{3c^5}|T|^2$$

$$I_{EQ} = \frac{\omega^6}{5c^5}\sum|EQ_{\alpha\beta}|^2$$

$$I_{MQ} = \frac{\omega^6}{20c^5}\sum|MQ_{\alpha\beta}|^2$$

Therefore, the total scattering intensity of the metasurface can be expressed as:

$$I = \frac{2\omega^4}{3c^3}|P|^2 + \frac{2\omega^4}{3c^3}|M|^2 + \frac{2\omega^6}{3c^5}|T|^2 + \frac{\omega^6}{5c^5}\sum|EQ_{\alpha\beta}|^2 + \frac{\omega^6}{40c^5}\sum|MQ_{\alpha\beta}|^2$$

S3. Spatial distribution of optical chirality enhancement

To better illustrate the spatial distribution of the superchiral field in the metasurface, we additionally plot the C_E at the resonance frequency on different cutting planes of the initial unit cell. from three cross-sections. With the substrate surface defined as the z=0 plane, Figure S2 shows the distribution of C_E under 135° linear polarization at z=1 μm (top of the dimer), and z=0 μm (substrate surface). It can be found that the sign of optical chirality enhancement is typically uniform across different cross-sections, and the higher C_E can be achieved at cut planes closer to the substrate surface. Moreover, strong superchiral field is concentrated around the dimer nanoresonators, which is accessible and advantageous for chiral sensing applications.[31]

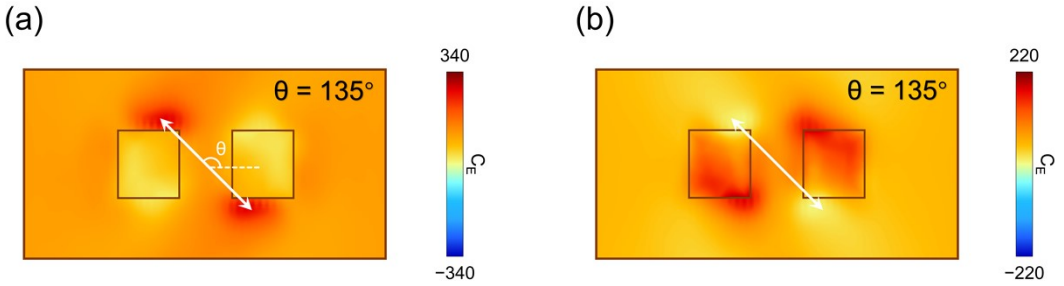

Figure S2. Distribution of C_E at the resonance frequency under 135° linear polarization at z=1 μm (a), and z=0 μm (b).

S4. Reflection spectra and the chirality enhancement of the metasurface with respect to *k* under CPL excitation

Circularly polarized waves can be decomposed into a combination of TE and TM polarized waves with ±π/2 phase difference. Therefore, the designed metasurface can support both electric and magnetic dipole modes under CPL excitation. Figure S3 illustrate the reflection spectra and C_{E_ave} with varying k and incident wavelengths. The metasurface exhibits the same reflection spectra under both RCP and LCP excitations, and the handedness of optical chirality is controlled by the excitation handedness. Compared to off-axis linear polarization excitation, the positions of the peak value of C_{E_ave} and the maximum reflectance do not coincide. However, the significant enhancement in volume-average optical chirality still indicates that the designed metasurface can generate strong chiral fields under circular polarization excitation.

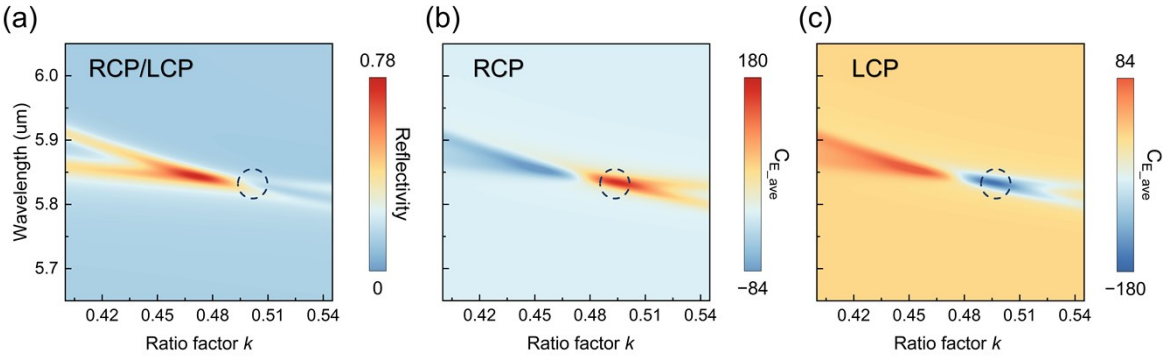

Figure S3. Reflection (a) and C_{E_ave} (b, c) spectra under CPL excitation with varying *k*. Dashed circles indicate the peak value of C_{E_ave}.

S5. Geometric parameters of the unit cell used for pixelated sensing approach

To measure molecular fingerprints, it is important to separate adjacent peaks of the vibrational absorption modes. Therefore, the full width at half maximum (FWHM) should be equal to or smaller than the minimum peak distance.[13] The FWHM of the metasurface is affected by the geometric parameters of the structure, especially on the distance *d* between the dimer. Moreover, the period aspect ratio *k* of the unit cell needs to be elaborately designed to ensure that each pixel can achieve the overlap of electric dipole and magnetic dipole modes. The value of geometric parameters scaled with *s* are described in table S1. In this work, we set k= -0.02+0.5s^{-2}, which is obtained by fitting an inverse quadratic function between *k* that satisfies the conditions of dipole overlapping and evenly chosen *s*, as shown in Figure S4a. In the design of proposed metasurface, we select the relationship between the geometric factor s and the geometric parameters through the following steps. Firstly, the resonance frequency of the metasurface depends on the unit cell periodicity and the geometric dimensions of the resonators. Therefore, we achieve broadband spectral coverage by designing a linear

relationship between the periodicity p_x, the resonator dimensions a and b, and the geometric factor s. The variation of d has little impact on the resonannce frequency, but it mainly affects the quality factor (Q) of the resonance. As a result, the distance between the dimer d is then used to adjust the asymmetric factor, which is chosen under the consideration that the more uniform Q and FWHM values are better suited for broadband spectral coverage detection. Finally, the selection of p_y is based on the period aspect ratio factor $k = p_x/p_y$, which ensures spectral overlap of electric and magnetic dipole modes. Figure S4b shows the FWHM and Q factor of the reflection spectra of all metapixels, and the extremely narrow linewidth meets the requirements for sensing resolution.

Table S1. Geometric parameters of the unit cell scaled with s

Geometric parameters	p_x	p_y	d	a	b
Value scaled with s [μm]	$5s$	$5k{\cdot}s$	s-0.3	$0.84s$	$0.72s$

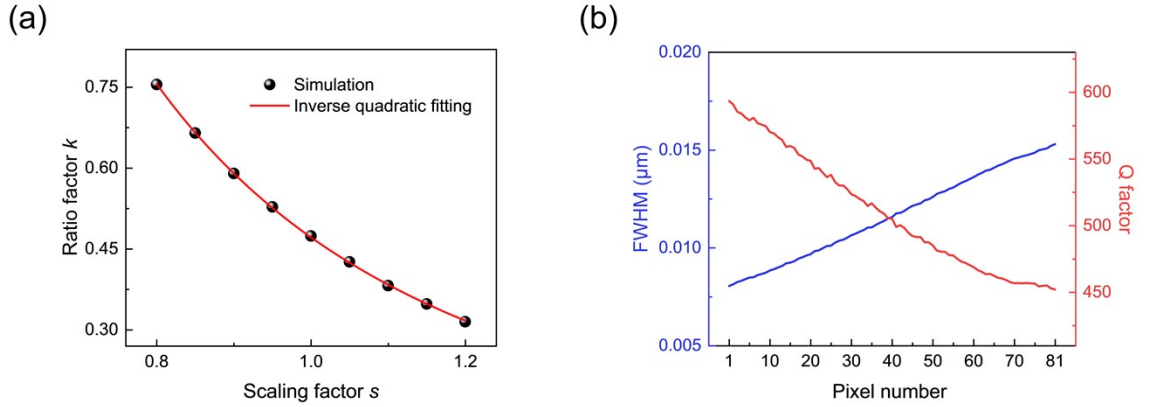

Figure S4. (a) Inverse quadratic fitting between k and s. (b) FWHM and Q factor of all metapixels.